High resolution 3D laser scanner measurements of a strike-slip fault quantify its morphological anisotropy at all scales

François Renard

Laboratoire de Géophysique Interne et Tectonophysique, Université de Grenoble, France & Physics of Geological Processes, University of Oslo, Norway

Christophe Voisin

Laboratoire de Géophysique Interne et Tectonophysique, Université de Grenoble, France

David Marsan

Laboratoire de Géophysique Interne et Tectonophysique, Université de Savoie, France

Jean Schmittbuhl

Ecole et Observatoire des Sciences de la Terre, Université de Strasbourg, France

Abstract. The surface roughness of a recently exhumed strike-slip fault has been measured by three independent 3D portable laser scanners. Digital elevation models of several fault surface areas, from 1 m^2 to 600 m^2, have been measured at a resolution ranging from 5 mm to 80 mm. Statistical scaling analyses show that the striated fault surface has a directional morphological anisotropy that can be described by two scaling roughness exponents, in two directions corresponding to the direction of slip and its perpendicular. A crossover length at the centimeter scale emerges from the two scaling regimes indicating that the anisotropy of the fault roughness should control the rupture propagation differently below and above this length scale.

1. Introduction

The roughness on active faults planes is supposed to concentrate the stress and therefore control earthquakes nucleation. Unfortunately, the small scale roughness cannot be imaged for faults at depth. Only high resolution relocalizations of earthquakes using the multiplet technique have shown earthquakes alignments along fault. This pattern was interpreted as resulting from the presence of an organized roughness (asperities) resisting the slip [Schaff et al. 2002].

The roughness of several faults planes has been studied using 1D profilometry [Power et al. 1987; Lee and Bruhn 1996] and it has been shown that normal fault surfaces contain ridges developing parallel to the direction of slip and holes elongated in a direction perpendicular to the slip. Moreover, the roughness is not isotropic and profiles parallel and perpendicular to the slip have different fractal dimensions.

It is not common to have access to exhumed fault planes with an important accumulated slip. For normal faults the vertical motion naturally builds fault scarps. Larger cumulated slips can be achieved on strike-slip faults but, as the vertical displacement is small, active fault scarps can seldom be observed. In this study, we have measured one of such fault

plane using different 3D field laser scanners and characterized its geometry in terms of scaling properties and anisotropy.
To add: Nucleation controlled by the small scales. Rupture arrest on barriers.

2. 3D scanner data

The Vuache fault, near Annecy in the French Alps (GPS coordinates: N 45°57.242', E 6°02.933'), was selected because the fault plane was exhumed only ~10 years ago by the activity of a quarry, and thus preserved from atmospheric alteration or glacier erosion. This is a 60x20 m strike-slip exhumed fault plane, in cretaceous limestones with decimeter horizontal bedding, and with a left-lateral cumulated slip of 2.3 km, and some minor right-lateral slips witnessed by several shear criteria on the fault plane. The fault is 30 km long. Striations at all scales on the fault plane, dipping at 35°, also indicate a strike-slip motion, with a small normal component. The striations are parallel to the bedding. The Vuache fault has broken at 16.5 km east from the measurement site the 15th of July 1996, leading to a M_L=5.3 earthquake located at 2 km depth [Thouvenot et al. 1998].
The fault surface was measured using three independent portable 3D laser scanners (Table 1). One device (S10) scans the surface by triangulation using a red laser and a camera. The other two devices (GS100, LMS Z420i) measure the time of flight of an infra-red reflected laser spot. Six sub-surfaces of the fault were scanned at various resolutions to cover surface scales from ~1 m^2 to 600 m^2 at a resolution from 5 mm to 80 mm, greater than the precision of the scanner.
The result is a cloud of points whose three-dimensional coordinates correspond to the points on the fault surface with a regular angular spacing (Figure 1, top). This 3D set of points is transformed into a 2+1D data set which corresponds to a Digital Elevation Model (DEM) over the mean plane of the fault (Figure 1, bottom). This step is done without any interpolation, by rotating the initial data cloud and subtracting a flat plane calculated by a two-dimensional least-squared method. This removes any planar tilt of the fault and the minimum elevation is set to zero. This new set of data is transformed into a regular spatial grid by undersampling the regular angular grid. This reduces the resolution of the fault scan, and it ensures that there is no interpolation between data points that could modify the statistical properties of the surface at large wavelengths. From the DEM data sets, 1D profiles can be extracted or the whole 2D surface can be directly analyzed using various statistical tools detailed below.

3. Surface roughness analysis

The roughness of the fault is studied by looking at how the distributions of height differences and slopes vary with the spatial wavelength. The aim is to demonstrate that the surface remains unchanged under the scaling transformation $\Delta x \to \lambda \Delta x$, $\Delta z \to \lambda^H \Delta z$ for 1D profiles extracted from the surface. For a self-affine profile, the Hurst exponent H lies in the range $0 \le H \le 1$. Moreover, as the surface is anisotropic because of the striation, the Hurst exponent might vary relative to the direction of slip.

A set of parallel cuts is taken through the digitized surface to obtain series of parallel profiles striking at an angle θ from the horizontal. A linear detrending is performed independently on all the profiles. The statistical properties of these 1D profiles are then calculated and averaged over a large number of parallel profiles. We also study how the scaling varies with θ, hence with their orientation relative to the direction of slip.

3.1. Height distribution

The distribution of heights $\delta z = \left| z_i - z_j \right|$, for two different intervals $I(\delta x)$ of $\delta\left(\left| x_i - x_j \right|\right) \in I(\delta x)$ is shown in Figure 2. It significantly departs from a Gaussian law, admitting large values much more frequently than a Gaussian model would predict, with a decay at large δz that roughly follows an exponential distribution. This feature is seen at all angles θ. The existence of exponentially distributed large heights implies that purely Gaussian models of the fault roughness would fail to capture the strongest geometrical asperities.

- Qu'est ce que ça veut dire en termes de physique de la striation ?

3.2. 1D analysis: root-mean-square correlation functions

A set of parallel profiles, with a constant orientation relative to the striation was extracted. For each profile, the root-mean square (RMS) correlation is calculated as a function of the spatial wavelength λ, and then averaged on all the 1D parallel profiles. For each window size λ, the RMS is averaged over the different positions of the window along the profile.

Self-affine profiles are defined over four decades by a single scaling behavior $f(\lambda) \propto \lambda^H$ where H is the Hurst exponent (Figure 3). H varies depending on the orientation of the profile relative to the direction of slip. Parallel to the striation, the Hurst exponent is equal to 0.58, and lower than the value close to 0.80 found for profiles oriented perpendicularly to the slip (Figure 4a).

Moreover, it is shown in Figure 4a that a crossover length scale exists at ~1 cm, where the RMS correlation value is the same for all profiles, whatever the orientation relative to the direction of slip.

3.3. 2D analysis: FFT and wavelets transform

In addition, 2D FFT were performed on each surface to verify the direction of anisotropy at all scales (Figure 5). In each case, this direction coincides with the striation visible on the DEM.

A more thorough 2D analysis of the anisotropy involves computing the best fitting planes $y = a_i x + b_i z + c$ centered on each point (x_i,y_i,z_i) of the fault, using a least-mean square method with a weight on point (x_j,y_j,z_j) following a Gaussian function $\exp(-r_{ij}^2/2L^2)$ where r_{ij} is the distance between the two points and L is the scale of observation. This then allows to estimate how the height RMS changes with distance, along any direction θ, without resorting to 1D cuts, by computing the

RMS of $L(a_i \cos\theta + b_i \sin\theta)$. Figure 6 shows this RMS for varying angles and scales, clearly exhibiting the changes in roughness with θ, the smoothest fault geometry obtained at an angle of nearly 50°. This confirms the presence of the anisotropy at all scales, down to the resolution of the scanner. There is no characteristic wavelength for the striation.
A vérifier avec David: quelle surface ? pourquoi 60° et pas 35°?

4. Discussion & conclusion

The angular variation of the Hurst exponent on the fault surface indicates that the fault is rougher in the direction of the slip (smaller Hurst exponent) than perpendicular to it. This observation has also been done at a smaller scale on experimental shear fractures [Amitrano and Schmittbuhl, 2002], where the Hurst exponent was H = 0.74 in the slip direction and H = 0.8 perpendicular to it. This is consistent with observations reported by *Power and Durham* [1997] and *Lee and Bruhn* [1996], and confirmed by our 3D data.
In addition, the two power laws of figure 3 cross at a specific length scale, at around 1 cm. Below this length scale, the fault surface is rougher in the direction of slip, and above this length scale, the fault is rougher in the direction perpendicular to the slip.
The direction of slip clearly appears on the 3D data, however, the statistical tools described here are not sufficient to determine whether the slip was left-lateral or right-lateral. This is a future challenge to develop stratistical tools that can target the asymmetry of the slip.

Acknowledgments. The project has been supported by the CNRS (ACI and DyETI program) and the University J. Fourier (BQR). We would like to thank J.-M. Nicole for his technical help, and F. Thouvenot, J.-P. Gratier, M. Bouchon, and G. Puaux for helpful discussions.

References

Amitrano, D., and J. Schmittbuhl, Fracture roughness and gouge distribution of a granite shear band, J. Geophys. Res., 107, 2375, 2002.
Barabási, A. L., and E. H. Stanley, Fractal concepts in surface growth, Cambridge Univ. Press, New York, 1995.
Hansen, A., J. Schmittbuhl, G. Batrouni, and F. D. Oliveira, Normal stress distribution of rough surfaces in contact, Geophys. Res. Lett., 27, 3639-3643, 2000.
Lee, J.-J., and R. Bruhn, Structural anisotropy of normal fault surfaces, J. Struc. Geol., 18, 1043-1059, 1996.
Meakin, P., Fractals: scaling and growth far from equilibrium, Cambridge Univ. Press, New York, 1998.
Mehrabi, A. R., H. Rassamdana, and M. Sahimi, Characterization of long-range correlations in complex distributions and profiles, Phys. Rev. E, 56, 712-722, 1997.
Power, W. L., T. E. Tullis, S. R. Brown, G. N. Boitnott and C. H. Scholz, Roughness of natural fault surfaces, Geophys. Res. Lett., 14, 29-32, 1987.
Power, W. L., and T. E. Tullis, Euclidean and fractal models for the description of rock surface roughness, J. Geophys. Res., 96, 415-424, 1991.
Schaff, D., G. H. R. Bokelmann, G. C. Beroza, F. Waldhauser, and W. L. Ellsworth, High resolution image of Calaveras fault seismicity, J. Geophys. Res., 107, 633-668, 2002.

Schmittbuhl, J., S. Gentier, and S. Roux, Field measurements of the roughness of fault surfaces, Geophys. Res. Lett., 20, 639-641, 1993.

Simonsen, I., A. Hansen, and O. M. Nes, Using wavelet transforms for Hurst exponent determination, Phys. Rev. E, 58, 2779-2787, 1998.

Thouvenot, F., J. Fréchet, P. Tapponnier, J. C. Thomas, B. Le Brun,, G. Ménard, R. Lacassin, L. Jenatton, J.R. Grasso, O. Coutant, A. Paul, and D. Hatzfeld, The M_L 5.3 Epagny (French Alps) earthquake of 1996 July 15: a long-awaited event on the Vuache Fault, Geophys. J. Int., 135, 876-892, 1998.

David Marsan, Laboratoire de Géophysique Interne et Tectonophysique, Université de Savoie, 73376 Le Bourget du Lac Cedex, France

François Renard & Christophe Voisin, Laboratoire de Géophysique Interne et Tectonophysique, BP 53, 38041 Grenoble, France

Jean Schmittbuhl, Institut de Physique du Globe de Strasbourg, 5 rue René Descartes, 67084 Strasbourg cedex, France

(Received September XX, 2005; revised September XX, 2005; accepted September XX, 2005.)

Paper number 2005GLXXXXXX.
0094-8276/01/2005GLXXXXXX$05.00

Paper number 2005GLXXXXXX.

Published in 2001 by the American Geophysical Union.

Paper number 2005GLXXXXXX.

Figures & Table

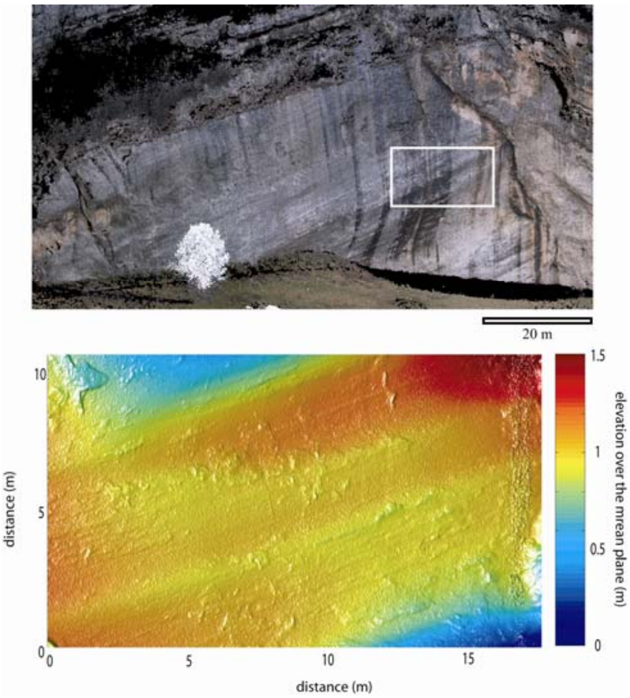

Figure 1. Scanner 3D data of the Vuache exhumed fault surface. Top: whole outcrop view. The inset corresponds to the bottom surface. Bottom: Zoom on the fault. The striation, with maximum amplitude of around 1 m, can be detected at all scales up to the resolution of the measurement. The surface contains 495,000 points, on a constant grid of 2cmx2cm. The resolution of the elevation measurement is 1 cm.

Figure 1. XX.

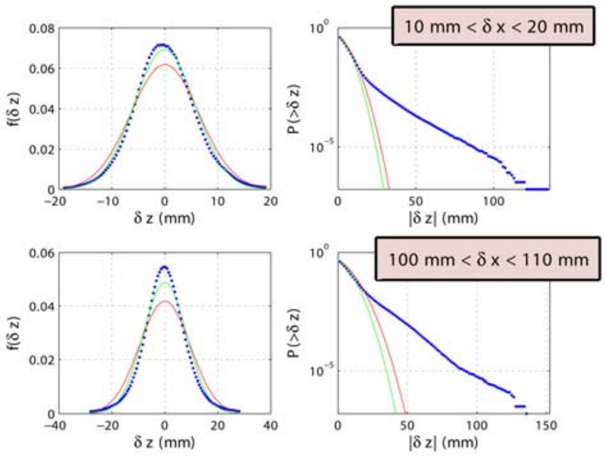

Figure 2. Left: Distribution of the heights δz for two intervals of δx=10-20 mm (top) and 100-110 mm (bottom), for θ=30°, in blue. Right: logarithm of the probability of exceedence, clearly showing the exponential decay of the distribution. Red: best gaussian fit, for the whole distribution. Green: best gaussian fit, for δz within 3 standard deviations of its mean.

Most the heights δz appear to follow the reduced gaussian fit (green), but with clear departure at large absolute values $|\delta z$.

Figure 2. XX.

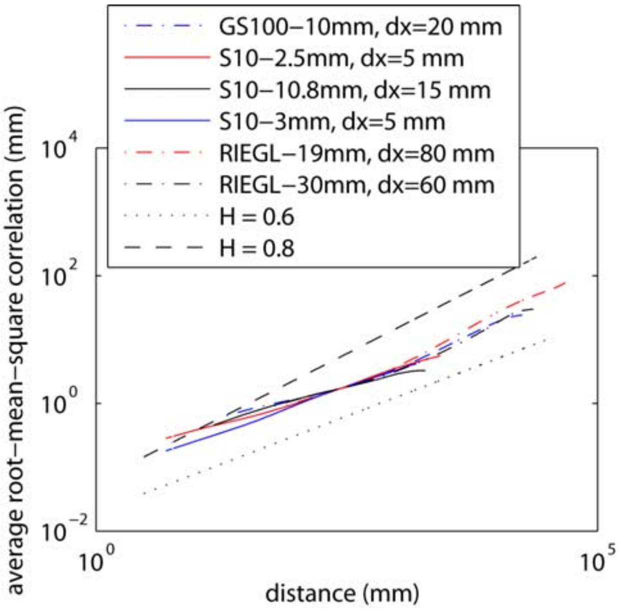

Figure 3. Root-mean-square correlation function of the fault surface. The resolution of acquisition is given as well as the under-sampled frequency *dx*.

Figure 3. XX

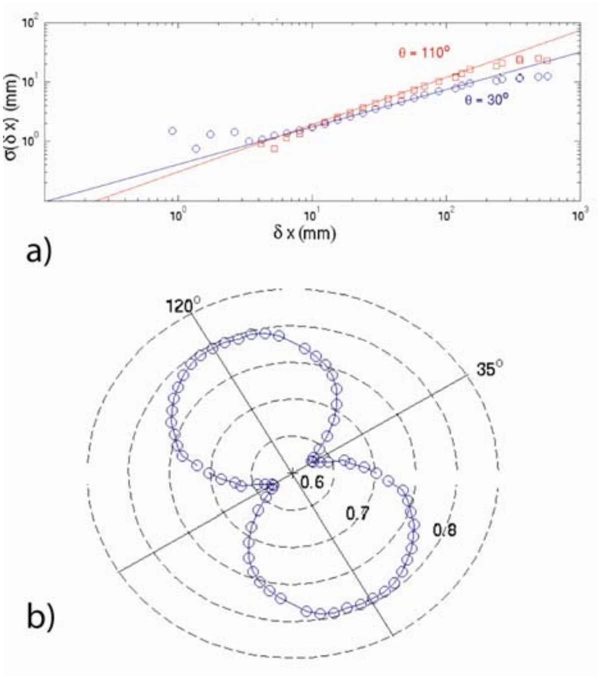

Figure 4. Anisotropy of the surface revealed by the angular variation of the Hurst exponent. A) RMS as a function of the distance along two profiles in the direction of the striation (30°) and perpendicular to it, showing the variation of the Hurst exponent. B) The minimum Hurst exponent (H=0.58) is at 35°, in the direction of the slip, and the maximum (H = 0.8) is in a perpendicular direction.

Figure 4. XX.

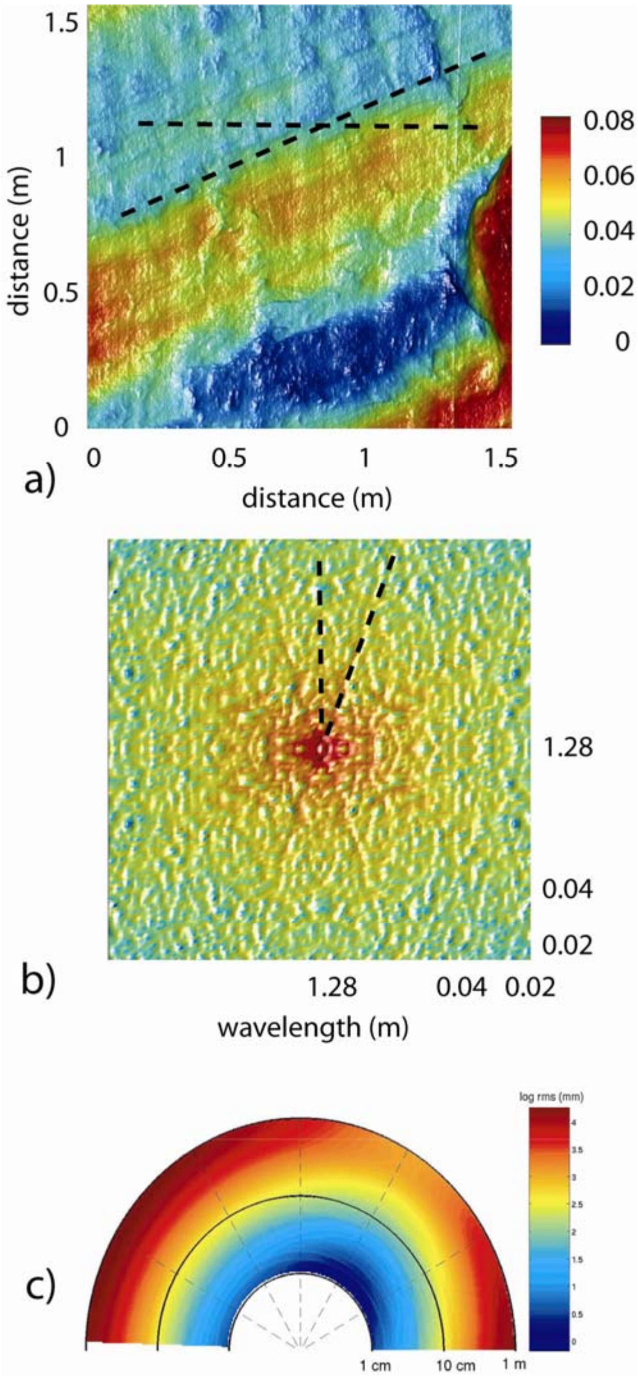

Figure 5. Anisotropy of the surface revealed by 2D analysis. a) DEM of the surface at a resolution of 5 mm. The dashed lines give the angle of the striation relative to the horizontal. b) 2D Fast-Fourier-Transform (FFT) showing the main direction of anisotropy of the surface. Again, the two dashed lines give the same angle as in a). c) RMS of the heights δy resulting from a 2D gaussian wavelet analysis for scales between 1cm and 1m, at various angles from the horizontal. The direction of slip is detected by the increase of RMS at an angle of 60°. For

both analysis, the anisotropy is detected at all scales for wavelength between 0.04 m and 1.28 m.

Figure 5. XX.

Table 1. 3D scanners characteristics.

3D scanner device	S10	GS100	LMS Z420i
Company	©TRIMBLE	©TRIMBLE	©RIEGL
Resolution	0.93 mm	13 mm	10 mm
Acquisition speed	70 pts/s	5000 pts/s	5000 pts/s
Data recovery	99%[1]	> 99.5%	> 99.5%

[1]The measurements were performed during the night to avoid interferences with the sun light.